Organic-based microcavities with vibronic progressions: Linear spectroscopy

L. Fontanesi*
Institute of Theoretical Physics, Ecole Polytechnique Fédérale de Lausanne (EPFL), CH-1015 Lausanne, Switzerland

L. Mazza
Max-Planck-Institut für Quantenoptik, Hans-Kopfermann-Straße 1, D-85748 Garching, Germany
and Scuola Normale Superiore, Piazza dei Cavalieri 7, I-56126 Pisa, Italy

G. C. La Rocca
Scuola Normale Superiore and CNISM, Piazza dei Cavalieri 7, I-56126 Pisa, Italy
(Received 8 July 2009; published 15 December 2009)

In this work we study from a theoretical point of view microcavities embedding organic materials featuring vibronic progressions. As already shown in seminal experiments, the presence of vibronic replicas largely enriches the physics of such systems with the appearance of new polariton dispersion branches. We calculate the linear optical properties of such microcavities using two distinct models, quantum the first, macroscopic the latter, which are fully consistent with each another. They are shown to describe the strong-coupling regime in very good agreement with the available experimental data, using independently determined material parameters.

DOI: 10.1103/PhysRevB.80.235313 PACS number(s): 71.36.+c, 78.20.Bh, 42.70.Jk

I. INTRODUCTION

The regime of strong light-matter coupling in monolithic inorganic semiconductor-based microcavities has been intensively studied up to the recent observation of Bose-Einstein condensation of cavity polaritons.[1] The achievement of a large value for the Rabi splitting is beneficial to the observation of strong-coupling features even at room temperature and has motivated the search of novel configurations and material combinations, e.g., from GaAs to CdTe to GaN or ZnO based microcavities.

Rather than focusing on inorganic semiconductors, an alternative line of research has considered microcavities based on organic semiconducting materials[2,3] as a viable route to very large Rabi splitting values. The first experimental proof of strong coupling in organic-based microcavities has been performed using disordered mixtures of J aggregates in a host matrix,[4] a system whose optical properties have been then broadly investigated, both experimentally and theoretically.[5–8] More recently, a new research line has focused the attention on polycrystalline and crystalline materials. These materials mainly differ from those previously studied for two features: on one hand vibronic resonances play a major role in the linear optical properties of the microcavity, up to the creation of additional polariton dispersion relations;[9] on the other hand the ordered crystalline structure allows the observation of a variety of phenomena arising from the strong optical anisotropy of these samples.[10–12] A new major experimental progress has been achieved with the growth of single-crystal organic microcavities,[13,14] where the measure of the polarization dependence of the linear optical properties has been possible. Furthermore, in Refs. 13 and 15 the first photoluminescence measures for crystalline samples have been reported.

In this paper we focus mainly on the influence of vibronic replicas on the physics of strongly coupled microcavities. Motivated by the experimental measures shown in Ref. 9, we build two general models, quantum the former and macroscopic the latter, explaining the multiple resonances in terms of a single electronic transition assisted by vibrational quanta. Both these models reproduce the experimental results.[16,17] In our analysis we will also take into account the anisotropic character typical of organic materials and simulate systems involving an arbitrary number of vibronic replicas with one molecule per unit cell. A second paper discussing the photoluminescence properties of such heterostructures will follow.[18]

This paper is organized as follows. In Sec. II the two models are explained each one with a descriptive example; the simulations of the experimental results are shown and discussed. Our conclusions are presented in Sec. III.

II. LINEAR OPTICS

Organic molecules in the solid phase tend to regularly arrange forming molecular crystals held together by van der Waals forces with binding energies much weaker than those due to covalent chemical bonds. In general, the intramolecular dynamics becomes relevant and the coupling of the electronic degrees of freedom to those of the nuclear structural backbone of a molecule cannot be neglected. Therefore we will use the Franck-Condon model,[19] widely adopted in solid-state physics to link an electronic transition to the modification in the nuclear configuration. We model a molecule as a simple two-level system whose ground state and lowest excited one have slightly different structural configurations. These two electronic levels can be represented as two adiabatic surfaces with equilibrium configurations displaced by a distance R_0 and having different energies. In this model we assume that one parameter is enough to describe the changes in the nuclear spatial configurations. The nuclear states are modeled as one-dimensional harmonic oscillators of mass M. An optical transition consists of an electronic and

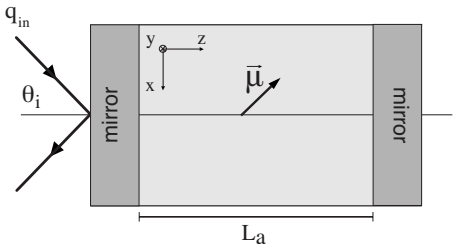

FIG. 1. Sketch of the system geometry: an organic resonant material of length L_a, with dipole moment $\boldsymbol{\mu}$, is embedded in a microcavity. The optical properties of such a system are investigated with reflectivity experiments.

a vibrational excitation: considering the Born-Oppenheimer approximation,[20] we can factorize the generic vibronic wave function in an electronic part and a nuclear one. The Franck-Condon principle states that an electronic transition is most likely to occur without changes in the positions of the nuclei, or, to put it better, that the transition dipole moment is proportional to the squared overlap of the vibrational wave functions. The transition probability takes the form

$$P_{a\mu\to b\nu} \propto |\langle\psi_b|e\mathbf{r}|\psi_a\rangle|^2|\langle\chi_{b\nu}|\chi_{a\mu}\rangle|^2, \tag{1}$$

where ψ_a identifies the ath electronic state while $\chi_{a\nu}$ represent the νth vibrational wave function of the ath electronic level. Calculating the overlaps at zero temperature we obtain the transition probabilities from the vibronic ground state, proportional to the oscillator strengths. They are modulated by a Poisson distribution,

$$P_{G0\to E\nu} \propto \frac{S^\nu}{\nu!}e^{-S}, \tag{2}$$

where G and E stand for ground and excited states and with

$$S\hbar\omega = M\omega^2 R_0^2/2, \tag{3}$$

where S is the Huang-Rhys parameter which takes the meaning of the average number of phonons accompanying the optical transition. At finite temperature, taking into account a population of the initial state that follows a Boltzmann distribution, these absorption peaks are modulated by a Laguerre distribution,[21] and if $\hbar\omega \gg k_B T$, as it is the case at room temperature, the previous results are approximately still valid. From now on the oscillator strength of the transition will be distributed among the vibronic replicas according to the modulation given by the previous equations.

A. Microscopic model

We have built a quantum model to describe light-matter interaction in microcavities containing anisotropic organic molecular crystal as resonant material.[12] The geometry of the generic system considered is shown in Fig. 1 where an organic slab, with a resonant dipole moment $\boldsymbol{\mu}$, is embedded between two mirrors separated by a distance L_a. Planar microcavities are formed by facing mirrors so as to quantize the electromagnetic field along the growth direction, the z axis in the examples considered, and to confine it on a plane: the eigenstates are represented by cavity photons. For each in-plane wave vector there are two possible polarizations, p (electric field vector parallel to the plane of incidence) and s (electric field vector perpendicular to the plane of incidence). We will consider only one relevant cavity mode energy with the dispersion relation

$$\hbar\omega_{\mathbf{q}} = \frac{\hbar c}{\sqrt{\varepsilon}}\sqrt{q^2 + \frac{\pi^2}{L_{eff}^2}}, \tag{4}$$

where q is the in-plane wave vector, L_{eff} is the effective length of the cavity, and ε is the background dielectric constant. In realistic cases polarization splitting[22] and penetration depth[23] should be taken into account, mainly when one has to deal with dielectric mirrors, but each case should be analyzed according to mirrors details and parameters.

The optical analysis is performed varying the incident light wave vector via angle tuning experiment, where the incident angle, θ_i, is connected to the in-plane wave vector, q, by the relation

$$q = \frac{E(q)}{\hbar c}\sin\,\theta_i, \tag{5}$$

where $E(q)$ is the energy of the incident photons.

Electronic excitations in molecular crystals are Frenkel excitons and their Hamiltonian can be written, in the Heitler-London approximation, considering a low exciton density,

$$H_{ex} = \sum_j \sum_{\mathbf{n}} \hbar\omega_j b_{j,\mathbf{n}}^\dagger b_{j,\mathbf{n}} + \sum_j \sum_l \sum_{\mathbf{n}\neq\mathbf{m}} J_{jl}(\mathbf{m}-\mathbf{n}) b_{j,\mathbf{n}}^\dagger b_{l,\mathbf{m}}, \tag{6}$$

where $b_{j,\mathbf{n}}^\dagger$ and $b_{j,\mathbf{n}}$ are, respectively, the composite creation and annihilation operators of an electronic excitation accompanied by j vibronic replicas at the molecule at site $\mathbf{n}$. On different sites $\mathbf{n}\neq\mathbf{m}$, they commute

$$[b_{i,\mathbf{n}}, b_{j,\mathbf{m}}^\dagger] = [b_{i,\mathbf{n}}, b_{j,\mathbf{m}}] = [b_{i,\mathbf{n}}^\dagger, b_{j,\mathbf{m}}^\dagger] = 0, \tag{7}$$

while on the same site they do not have a definite statistics as the electronic operators (paulions) anticommute, while the vibrational ones (bosons) commute.

ω_j takes account of the independent molecule frequency transition and of the gas to solid molecule frequency shift[3,24,25] and increases linearly in j,

$$\omega_j = \omega_0 + j\omega_{01}, \quad \omega_{01} \ll \omega_0, \tag{8}$$

where ω_{01} is the energy associated to the vibronic transition. The second sum in Eq. (6) takes into account the excitation transfer between molecules; the interaction parameter representing dipole-dipole coupling between two molecules at sites $\mathbf{n}$ and $\mathbf{m}$ is also effective between states with different numbers of vibrational replicas ($j\neq l$),

$$J_{jl}(\mathbf{m}-\mathbf{n}) = \langle\chi_{e,j}|\chi_{g,0}\rangle\langle\chi_{g,0}|\chi_{e,l}\rangle\tilde{J}(\mathbf{m}-\mathbf{n}). \tag{9}$$

The periodic structure of a lattice allows us to diagonalize the excitonic Hamiltonian defining the operators,

$$b_{j,\mathbf{k}}^{\dagger} = \sqrt{\frac{2}{M(N+1)}} \sum_{\mathbf{n}} \sin(k_z n_z) e^{i\mathbf{k}\cdot\mathbf{n}} b_{j,\mathbf{n}}^{\dagger}, \tag{10}$$

where M is the number of unit cells in the plane, N is the number of parallel planes, k_z is the wave vector in the z direction, and n_z denotes the location of a monolayer on the z axis. This Hamiltonian, that now takes the form

$$H_{ex} = \sum_{\mathbf{k}} H_{ex\mathbf{k}} = \sum_{\mathbf{k}} \sum_{j} \sum_{l} E_{jl}(\mathbf{k}) b_{j,\mathbf{k}}^{\dagger} b_{l,\mathbf{k}}, \tag{11}$$

can be easily diagonalized by operators that are linear combinations of the $b_{j,\mathbf{k}}^{\dagger}$; in the limit of low excitation these operators can be regarded as bosons.[3,25] Typically the intermolecular interactions are small and these delocalized states are almost dispersionless.

The coupling of excitons and cavity photons is described within the dipole approximation so that the interaction is $V = -\boldsymbol{\mu}\cdot\mathbf{E}$, where $\boldsymbol{\mu}$ is the dipole moment operator of the organic material and $\mathbf{E}$ is the cavity electric field operator. In this case we consider only transitions starting from the ground state without any vibronic replica: the oscillator strength of the electronic transition is distributed over a few transitions to the excited state distinguished by the number of vibrational quanta accompanying the transition. Absorption processes involving vibronic replicas at the ground state have a negligible weight at room temperature and will not be considered. On the other hand these states have a crucial role in the relaxation dynamics, thus they have to be taken into account in the study of the photoluminescence.[17,18]

The Hamiltonian of this system, in the linear coupling regime, takes the form

$$H = \sum_{\mathbf{k}} \left[H_{ex\mathbf{k}} + \sum_{\lambda=s,p} \hbar\omega_{\mathbf{k}} a_{\lambda,\mathbf{k}}^{\dagger} a_{\lambda,\mathbf{k}} + \sum_{j} \sum_{\lambda=s,p} (g_{j\lambda\mathbf{k}} b_{j,\mathbf{k}}^{\dagger} a_{\lambda,\mathbf{k}} + g_{j\lambda\mathbf{k}}^{*} b_{j,\mathbf{k}} a_{\lambda,\mathbf{k}}^{\dagger}) \right], \tag{12}$$

where $\mathbf{k}$ is the in-plane wave vector and $a_{\lambda,\mathbf{k}}^{\dagger}$ is the creation operator of the cavity photon λ polarized. Interaction elements, $g_{j\lambda\mathbf{k}} = G_{j\mathbf{k}} P_{\lambda}$, are proportional to the square roots of the partitioned oscillator strengths, in fact

$$G_{j\mathbf{k}} = i \sqrt{\frac{4\hbar\omega_{\mathbf{k}}}{LA\varepsilon}} \sqrt{\frac{4M(N+1)}{\pi}} \sqrt{\frac{S^j}{j!}\frac{e^{-S}}{\mathcal{N}}}, \tag{13}$$

where L is the spacing between the mirrors and A is the quantization area; $\mathcal{N}$ is a normalization factor taking into account that we usually consider only a finite number of resonances. In the dipole approximation the $g_{j\lambda\mathbf{k}}$ polarization dependence (P_{λ}) can be calculated with simple geometrical considerations: considering a generic dipole moment along the cavity plane, $\boldsymbol{\mu} = (\mu_x, \mu_y, 0)$, and defining the two unit vectors, $\hat{\mathbf{n}}$ and $\hat{\mathbf{e}}$, in directions perpendicular and parallel to the in-plane wave vector which forms an angle ϕ with the x axis, the coupling parameters read

$$g_{js\mathbf{k}} = G_{j\mathbf{k}} \boldsymbol{\mu}\cdot\hat{\mathbf{n}}, \quad g_{jp\mathbf{k}} = G_{j\mathbf{k}} \sqrt{1 - \frac{k^2}{Q^2}} \boldsymbol{\mu}\cdot\hat{\mathbf{e}}, \tag{14}$$

and replacing the values of the unit vectors

$$g_{js\mathbf{k}} = G_{j\mathbf{k}}(-\mu_x \sin\phi + \mu_y \cos\phi),$$

$$g_{jp\mathbf{k}} = G_{j\mathbf{k}} \sqrt{1 - \frac{k^2}{Q^2}} (\mu_x \cos\phi + \mu_y \sin\phi), \tag{15}$$

where $Q = \sqrt{k^2 + k_z^2}$ is the total wave vector.

The Hamiltonian built so far can be diagonalized to obtain the polariton dispersion relations and the relative polariton operator

$$A_{\mathbf{k}}^{t} = X_{s\mathbf{k}}^{t} a_{s,\mathbf{k}} + X_{p\mathbf{k}}^{t} a_{p,\mathbf{k}} + \sum_{j} X_{j\mathbf{k}}^{t} b_{j,\mathbf{k}}, \tag{16}$$

where X's represent the relative components in the linear picture and t labels the polariton branch.

The optical properties of the system are investigated coupling these internal modes with the external fields applying the quasimode formalism.[23] Nonideal mirrors allow coupling between internal eigenstates and the continuum of fields on both sides with the same in-plane wave vectors and polarizations. Internal eigenstates are derived by means of the method outlined previously whereas the continuum of external fields can be described by the Hamiltonian,

$$H_r = \sum_{\mathbf{k}\lambda} \int d\omega_{\mathbf{k}} \hbar\omega_{\mathbf{k}} d_{\lambda,\mathbf{k}}^{\dagger}(\omega_{\mathbf{k}}) d_{\lambda,\mathbf{k}}(\omega_{\mathbf{k}}), \tag{17}$$

where $d_{\lambda,\mathbf{k}}^{\dagger}$ is the creation operator of an external mode on the right side and the same can be done for the left one, defining the creation operator $c_{\lambda,\mathbf{k}}^{\dagger}$. The coupling elements can be written

$$V = i \sum_{\mathbf{k}\lambda} \int d\omega_{\mathbf{k}} \hbar u_r(\omega_{\mathbf{k}}) [a_{\lambda,\mathbf{k}} d_{\lambda,\mathbf{k}}^{\dagger}(\omega_{\mathbf{k}}) - d_{\lambda,\mathbf{k}}(\omega_{\mathbf{k}}) a_{\lambda,\mathbf{k}}^{\dagger}] + i \sum_{\lambda,\mathbf{k}} \int d\omega_{\mathbf{k}} \hbar u_l(\omega_{\mathbf{k}}) [a_{\lambda,\mathbf{k}} c_{\lambda,\mathbf{k}}^{\dagger}(\omega_{\mathbf{k}}) - c_{\lambda,\mathbf{k}}(\omega_{\mathbf{k}}) a_{\lambda,\mathbf{k}}^{\dagger}], \tag{18}$$

where u_r and u_l are the right and left coupling parameters that, in good approximation, are connected[23] with the reflectivity R_j of the high-quality mirrors by $u_j^2(\omega) = \frac{\gamma_{phi}}{2\pi} = \frac{c(1-R_j)}{4\pi\sqrt{\varepsilon}L}$, with $j = l, r$. We assume these coupling parameters as constant in the investigated energy range. The equations of motion for the external fields and the polariton states can be solved for each value of the in-plane wave vector, so for a fixed $\mathbf{k}$ they are

$$\frac{d}{dt} c_{\lambda}(\omega) = -i\omega c_{\lambda}(\omega) + u_l \sum_{t} X_{\lambda}^{t*} A^{t},$$

$$\frac{d}{dt} d_{\lambda}(\omega) = -i\omega d_{\lambda}(\omega) + u_r \sum_{t} X_{\lambda}^{t*} A^{t},$$

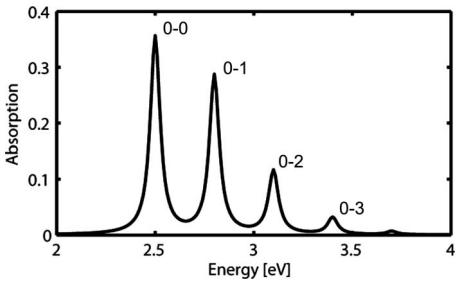

FIG. 2. Simulated absorption spectrum of a hypothetical bare 260-nm-thick film.

$$\frac{d}{dt}A^t = -i\Omega_t A^t - \sum_{\lambda} \int d\omega X_{\lambda}^t [u_r(\omega)d_{\lambda}(\omega) + u_l(\omega)c_{\lambda}(\omega)], \tag{19}$$

where t identifies the polariton state, Ω_t is the tth polariton eigenvalue and the cavity-mode operators, a_{λ}, have been represented in terms of the polaritons operators A^t. We have included phenomenologically the absorption of the active medium via damping rates in the exciton replicas frequencies so that complex excitonic frequencies are considered ($\omega_j^{ex} \rightarrow \omega_j^{ex} - i\gamma_{exc,j}$). Optical parameters can be obtained once a given input field is specified:[12] they are directly correlated with the photonic components of the polariton modes and can be expressed in terms of the matrix elements constituted with these components

$$\Lambda_{\lambda\nu} = \sum_t \frac{X_{\lambda}^t X_{\nu}^{t*}}{\omega - \Omega_t}, \tag{20}$$

where the subscripts stand for the polarization states.

Our optical analysis is polarization dependent so it is also appropriate for anisotropic systems showing polarization mixing. With this microscopic model we analyze an example of an anisotropic material embedded in a microcavity so as to study the optical properties and to highlight the features of this model. We consider a 260-nm-thick active material ($\varepsilon = 1$) whose absorption spectrum is reported in Fig. 2, with a transition energy of 2.5 eV and vibrational quanta with energy 0.3 eV, with a Huang-Rhys parameter of 0.8 so to distinguish various resonances. In addition we consider a generic anisotropic case with a dipole moment lying on a plane parallel to the mirrors and forming an angle $\pi/4$ with the plane of incidence. In order to operate in the strong-coupling regime, we chose a very narrow linewidth for every resonance ($\gamma_{exc} = 0.05$ eV) and highly reflecting mirrors ($\gamma_{pht} = 0.03$ eV). Figure 3 shows the s-polarized reflectivity spectrum with s-polarized incident light of such a layer (as in the presently available experimental spectra). The main features emphasized by these spectra are the dispersion relation: the anticrossing behavior of the lowest modes is evident but the anisotropy brings an additional cavity-photonlike mode that crosses all the polariton modes causing low reflectivity points. This phenomenology can be explained considering that the uniaxial symmetry leaves a free-propagation direction orthogonal to the dipole vector, this feature disappears in the isotropic case. An even more interesting peculiarity of

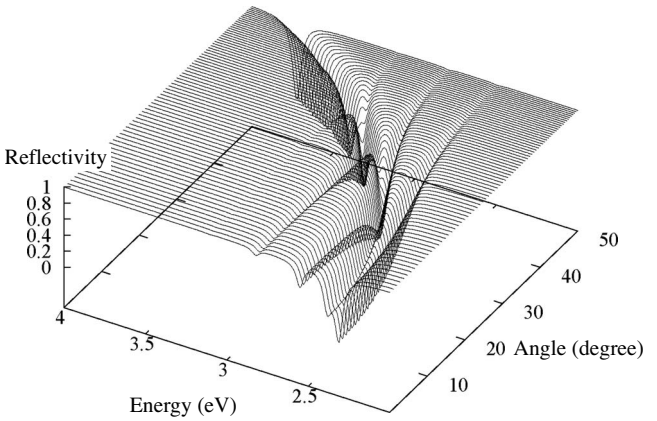

FIG. 3. Reflectivity s-polarized spectra with s-polarized incident light of the material embedded in a high-quality microcavity. This simulation has been performed with the microscopic model.

the anisotropy is the polarization mixing shown in Fig. 4, where the p-polarized transmission from s-polarized incident light is remarked. The intensity is particularly high on the resonant energies where the role of the dipole, and thus of the mixing, is stronger. The intensity of the mixed reflectivity depends strongly on the angle formed by the dipole with the incidence plane and disappears in the isotropic case.

B. Macroscopic model

A second approach exploited to compute the optical properties of the system consists in a macroscopic description of the microcavity. The starting point is the characterization of a dielectric function for the crystal slab that relates the electric displacement field $\mathbf{D}$ to the electric field $\mathbf{E}$, inside the material, according to the relation $\mathbf{D}_i = \Sigma_j \varepsilon_{ij} \mathbf{E}_j$. In the dipole approximation the generic dielectric tensor, ε_{ij}, has a uniaxial symmetry and in the coordinate system of the principal axes can be written in diagonal form as

$$\hat{\boldsymbol{\varepsilon}} = \begin{pmatrix} \varepsilon_{\parallel} & 0 & 0 \\ 0 & \varepsilon_{\perp} & 0 \\ 0 & 0 & \varepsilon_{\perp} \end{pmatrix} \tag{21}$$

with a dielectric function, along the resonant axis, of the form

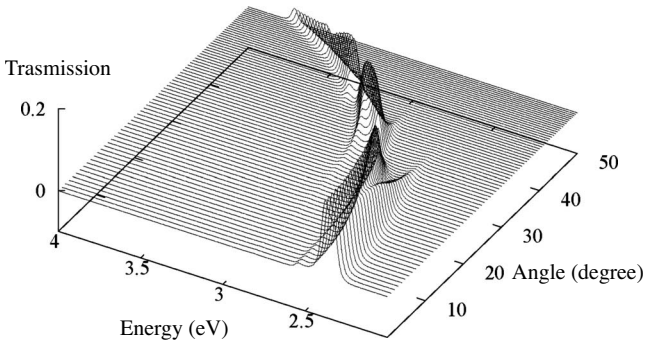

FIG. 4. Transmissivity p-polarized spectra with s-polarized incident light of the material embedded in a high-quality microcavity. This simulation has been performed with the microscopic model.

$$\varepsilon_{\parallel}(\omega) = \varepsilon_{\perp} + \frac{4\pi e^2}{m_0} \sum_{j}^{Res} \frac{f_j}{(\omega_j^2 - \omega^2 - 2i\omega\gamma_{exc,j})}, \quad (22)$$

where $\varepsilon_{\perp}$ accounts for the isotropic background, f_j are the oscillator strengths per unit volume distributed among the vibronic replicas as above, ω_j are the resonant energies, $\gamma_{exc,j}$ is the linewidth of each resonance, and the sum is over all the relevant resonances. With an arbitrary rotation a generic direction of the dipole moment can be obtained.

The optical analysis can be carried out solving Maxwell's equations for the given system with adequate boundary conditions. In order to set up a flexible algorithm, we use a transfer-matrix approach. The traditional approach for isotropic materials involves 2×2 matrices, but we adopt a 4×4 matrix method,[26,27] valid for layered anisotropic systems, which considers the electromagnetic field in his polarization modes, p and s. Considering an incident light with wave vector $\mathbf{k}_a$, the behavior of the electromagnetic wave inside each stratified medium can be described by a matrix that contains information about the ratio between incident, reflected, and transmitted wave amplitudes. In details, denoting with A_s, A_p, B_s, B_p, C_s, and C_p the complex amplitudes of, respectively, incident, reflected, and transmitted waves (the subscript denotes the polarization), we can define a 4×4 transfer matrix as

$$\begin{pmatrix} A_s \\ B_s \\ A_p \\ B_p \end{pmatrix} = \begin{pmatrix} T_{11} & T_{12} & T_{13} & T_{14} \\ T_{21} & T_{22} & T_{23} & T_{24} \\ T_{31} & T_{32} & T_{33} & T_{34} \\ T_{41} & T_{42} & T_{43} & T_{44} \end{pmatrix} \begin{pmatrix} C_s \\ 0 \\ C_p \\ 0 \end{pmatrix}, \quad (23)$$

where we have assumed there are no back traveling waves from the exit medium. If d_i is the thickness of the ith layer, an inverted partial transfer matrix, T_{ip}, can be defined, and the total transfer matrix takes the form

$$\mathbf{T} = \mathbf{L}_a^{-1} \prod_{i=1}^{N} \mathbf{T}_{ip}(-d_i)\mathbf{L}_f, \quad (24)$$

where $\mathbf{L}_a$ and $\mathbf{L}_f$ are the input and exit matrices that connect the p and s modes inside the stratified medium with those in the input and exit media. For further details on these matrices we refer to the Schubert's paper.[26] Eight transmission and reflection coefficients can be defined calculating the ratios between outgoing amplitudes and incident ones, and they can be expressed in terms of the matrix $\mathbf{T}$, such as, for instance, the s-polarized reflection coefficient with s-polarized incident light

$$r_{ss} = \left(\frac{B_s}{A_s}\right)_{A_p=0} = \frac{T_{21}T_{33} - T_{23}T_{31}}{T_{11}T_{33} - T_{13}T_{31}}. \quad (25)$$

According to generalized ellipsometry the complex reflectance ratio can be defined

$$\rho = \tan\Psi e^{i\Delta} = \left(\frac{B_p}{A_p}\right)\left(\frac{B_s}{A_s}\right)^{-1} \quad (26)$$

and can be expressed as a function of $\mathbf{T}$ and of the incident amplitudes. The basis of this approach is to define three linear independent normalized reflection matrix elements so that the optical parameters can be directly calculated.

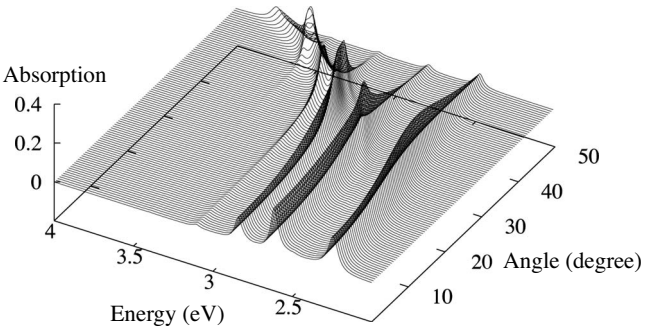

FIG. 5. Absorbtion spectra with s-polarized incident light of the material embedded in a high-quality microcavity. This simulation has been performed with the macroscopic model.

The calculation of the transfer matrix for anisotropic slabs moves from the first-order Maxwell's equations that can be written in matricial form

$$\frac{\partial}{\partial z}\psi(z) = ik_0\Delta(z)\psi(z), \quad (27)$$

where

$$\psi(z) = (E_x, E_y, H_x, H_y)^T(z), \quad k_0 = \frac{\omega}{c},$$

the 4×4 Δ matrix depends on the dielectric tensor and on the in-plane wave vectors components. If the medium is homogeneous Δ does not depend on z and we can formally write

$$\psi(z+d) = e^{i\omega/c\Delta d}\psi(z) = T_p\psi(z), \quad (28)$$

where all the multiple reflections are considered in a self-consistent way. The partial transfer matrix T_p can be determined in function of Δ applying the theorem of Cayley-Hamilton.[28]

It will now be investigated an example completely analogous to that of the previous section to compare the two models. The resonant material has been embedded between two highly reflecting distributed Bragg reflectors (DBRs) with two pairs of layers with refractive indices $n_1=1.3$ and $n_2=3.6$. The optical results given by this macroscopic analysis are completely consistent with the ones given by the quantum model. In Fig. 5 is shown the absorption spectra with s-polarized incident light: the several polariton modes are clearly evident as well as the strong absorptions close the anticrossing regions. This means that the cavity mode strongly couples to the resonance with no phonon as well as to the first phonon-assisted replicas. Since the absorption is a feature related to the resonance, and, in particular, to its linewidth, in this spectrum there is no mark of the noncoupled direction.

The two models presented so far are completely consistent, as it happens in absence of vibronic replicas.[23] An evidence of this agreement emerges from the comparison of the transmission spectra of Figs. 4 and 6 obtained with the two models. Clear analogies are shown by the two spectra for

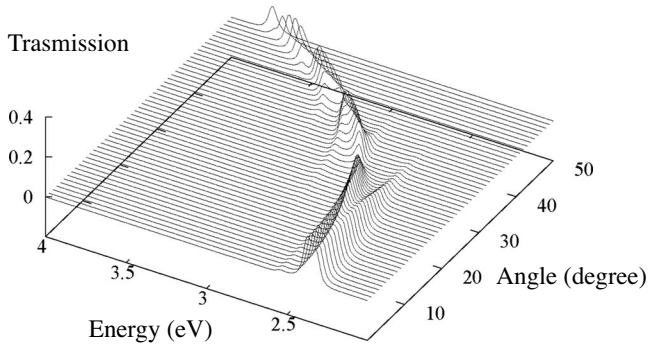

FIG. 6. Transmissivity *p*-polarized spectra with *s*-polarized incident light of the material embedded in a high-quality microcavity. This simulation has been performed with the macroscopic model.

what concern the amplitudes and the positions of the resonances. In both the figures it is evident the polarization mixing arising for values of the cavity photon resonating with the excitonic replicas. This behavior appears with a group of peaks for every excitonic transition (four of them are evident in Figs. 4 and 6) and the amplitude of the mixed transmission appreciably decreases at large angles in both the spectra. Some minor discrepancies arise from the simulations, they are mainly due to the different treatment of the photonic part of the problem. First of all the characterization of the mirrors: in both systems they are highly reflecting but while they are realistic DBRs in the macroscopic case, in the microscopic one the coupling to the external modes is directly computed from the value of the reflectivity. Another relevant phenomenon is the polarization splitting that is automatically accounted in the transfer-matrix method but has to be inserted by hand in the quantum case.

C. Simulation and results

The last part of this analysis concerns the simulation of the experimental results with the models explained so far and the comparison of the parameters with those obtained by Holmes and Forrest[9] reproducing the experimental dispersion relations. Since the absorbance spectrum of the bare 3,4,7,8 napthalenetetracarboxylic dianhydride (NTCDA) film [Fig. 7(a)] shows two different and narrow peaks, they fitted the reflectivity spectra with a simple three coupled oscillator

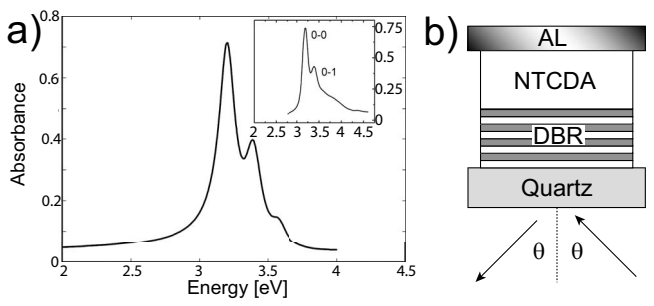

FIG. 7. (a) Simulated absorbance of a bare 50-nm-thick NTCDA slab. In the inset the experimental spectrum adapted from Ref. 9. (b) Experimental setup reproduced in the simulations.

model, coupling the cavity photon with two nondispersive exciton modes following

$$\begin{bmatrix} E_p & V_1 & V_2 \\ V_1 & E_{ex1} & 0 \\ V_2 & 0 & E_{ex2} \end{bmatrix}, \quad E_p = E_0\left(1 - \frac{\sin^2\theta}{n_{eff}^2}\right)^{-1/2}, \qquad (29)$$

where the two uncoupled transition energies, E_{ex1} and E_{ex2}, appear. V_1 and V_2 are the two interaction potentials, E_0 is the cutoff energy, θ is the incident angle, and n_{eff} is the effective refractive index. They adjusted four free parameters (V_1, V_2, E_0, and n_{eff}) to obtain a best fit to the experimental data.

In our simulation we start from the macroscopic model because it allows to reproduce exactly the experimental configuration without additional fitting parameters linked to mirrors reflectivity and polarization splitting. Since the investigated material is polycrystalline NTCDA, consisting of randomly oriented crystallites, we have adopted isotropic algorithms: a diagonal isotropic dielectric tensor in the macroscopic model, and a simpler three coupled oscillator model in the microscopic case with an angle-independent interaction and a single cavity mode. In this isotropic case the quantum model is similar to the model used by Holmes and Forrest to fit the experimental data. The simulation layout is arranged in order to have no additional free parameters to fit the strong-coupling regime, in fact we only use parameters obtained from the bare-material properties and from the experimental dielectric configuration. The first step is the setting of an appropriate dielectric tensor reproducing the known absorbance spectra of a bare 50-nm-thick slab of NTCDA with the transfer-matrix algorithm, so as to evaluate excitonic and phononic energies, the Huang-Rhys parameter and the oscillator strength. The experimental absorbance spectrum and the simulated one are shown in Fig. 7(a). This isotropic dielectric tensor is then used to calculate the optical reflection coefficients of the realistic system embedded in an asymmetrical microcavity [Fig. 7(b)]. This kind of microcavities, constituted of a dielectric and a metallic mirror are typically adopted for organic materials. The optical analysis has been performed on thermally evaporated polycrystalline NTCDA with thicknesses of 40 and 60 nm. In the simulations the mirrors have been reproduced according to tabulated data:[29] a DBR with eight pairs of alternating isotropic layers, constituted of SiO_2 ($n \sim 1.46$) and SiN_x ($n \sim 2$), deposited on a macroscopic quartz substrate and a 200-nm-thick aluminum mirror. A reflectivity analysis with *p*-polarized incident light on the quartz substrate has been performed on these sample via angle tuning experiments: also the simulations accounts for the relation between incident angle and in-plane wave vector to have analogous angle-dependent reflectivity data. The output of the first simulation are the reflectivity spectra reported in Fig. 8, this is done in analogy with the experimental results (also reported in Fig. 8). From this example it is clear that the simulated reflectivity spectra are in very good agreement with experimental ones both for what concerns the DBR sidebands and for the polariton states (pointed by arrows) that are well reproduced in their energy and in their linewidth. The

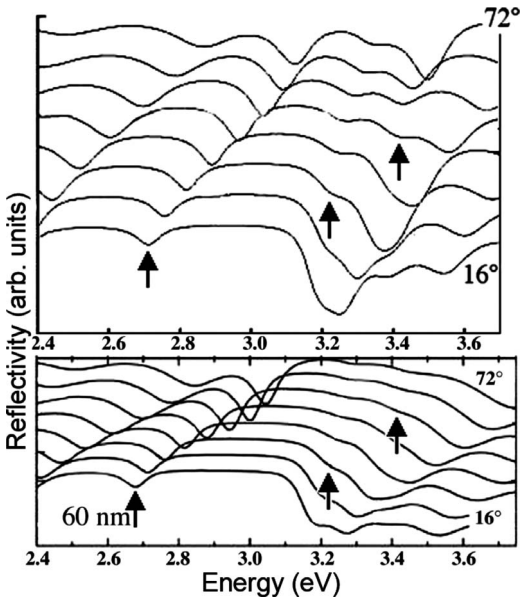

FIG. 8. Theoretical (upper) and experimental (lower), adapted from Ref. 9, reflectivity spectra for a 60-nm-thick slab of NTCDA in microcavity, obtained with *p*-polarized incident light. Spectra are plotted with an angular step of 8° and they are shifted for clarity.

consistence that appears from the comparison of the polaritons linewidths entails a correct description of the cavity mirrors, and hence of the photonic component.

From the minima of these spectra the polaritons dispersion relations can be obtained, as shown in Fig. 9. From this figure emerges that the cavity photon strongly couples to the two first vibronic transitions, as observed experimentally. For what concerns the 60-nm-thick slab, the main mismatch of this simulation with the data appears in the lower polariton, whose energy is a bit too high with respect to the experimental results, and in the upper polariton at large energies, where the photonic character is too pronounced. This feature is also more evident in the 40 nm case, where the predicted upper polariton at large angles is too dispersive. In both cases the explanation could be that the tabulated value used for the refractive index[30] is not accurate or appropriate for this case. As a matter of fact, Holmes and Forrest for their fit adjusted the refractive index as shown in Table I. In the last step of the simulation the optical reflectivity spectra obtained with the macroscopic model are reproduced with the corresponding microscopic approach to be able to compare the parameters with that obtained from the experimenters fit: this comparison is summarized in Table I.

TABLE I. Comparison of the parameters of the three coupled oscillator models [cf. Eq. (29)] fitted directly to experimental data (Ref. 9) and obtained from our simulations.

	40 nm		60 nm	
Thickness	Expt.	Sim.	Expt.	Sim.
E_0 (eV)	2.88 ± 0.05	3.05	2.70 ± 0.05	2.82
n	1.6	1.61	1.8	1.61
V_1 (meV)	140 ± 10	110	180 ± 10	160
V_2 (meV)	50 ± 10	50	60 ± 10	70

It can be seen that the main mismatches are in the coupling parameter V_1 and in the cavity photon energy E_0, larger than the experimental one; this stresses and confirms the differences found in the 60 nm case. All our results are obtained starting only from bare materials features and experimental configuration data, without adjusting free parameters in the strong-coupling regime.

This procedure is also suitable for the recent results obtained with single-crystal organic microcavities.[13] The main modification would be the adoption of an appropriate biaxial dielectric function.

III. CONCLUSIONS

We have developed two consistent models for the study of light-matter interaction in microcavities containing organic materials with vibronic replicas. The results of these models generalize those previously obtained without vibronic progressions.[2,6–8,11,12,27] Moreover the dispersion relations and the optical spectra of the first experimental results[9] with coupling to different vibronic replicas are well reproduced without using additional free parameters to fit the strong-coupling regime. The most interesting behaviors emerging from the simulations are linked to the anisotropy of the sys-

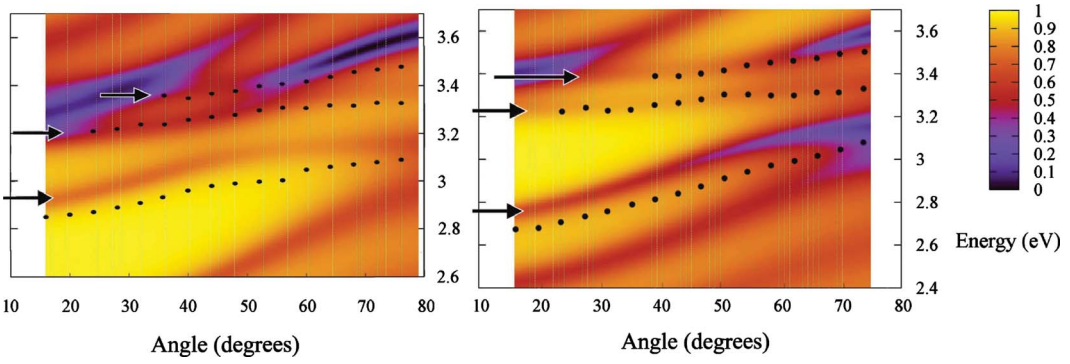

FIG. 9. (Color online) Reflectivity spectra (linear color scale) vs angle and energy. These plot show the dispersion relations obtained from reflectivity spectra for the 40-nm-thick (left) and 60-nm-thick (right) NTCDA slabs. Theoretical dispersion curves are the minima of darker areas pointed by arrows while experimental ones are shown as spots. At lower and higher energies are evident DBR sidebands.

tem, one of the main differences with respect to inorganic semiconductor microcavities. Therefore these models could be a powerful instrument of calculation and inspection of the optical properties of organic-based microcavity systems, mainly in the light of the recent achievements realized with single-crystal microcavities.[10,13] A further study on the photoluminescence of such microcavities will be published soon.[18]

ACKNOWLEDGMENTS

We would like to thank Leonardo Silvestri, Hashem Zoubi, Paolo Michetti, Vincenzo Savona for fruitful discussions and comments on this work during its preparation. We gratefully acknowledge support of the European Commission via Grant No. FP7-PEOPLE-ITN-2008-237900 "ICARUS."

*luca.fontanesi@epfl.ch

[1] J. Kasprzak, M. Richard, S. Kundermann, A. Baas, P. Jeambrun, J. M. J. Keeling, F. M. Marchetti, M. H. Szymańska, R. André, J. L. Staehli, V. Savona, P. B. Littlewood, B. Deveaud, and L. S. Dang, Nature (London) **443**, 409 (2006).
[2] V. Agranovich, H. Benisty, and C. Weisbuch, Solid State Commun. **102**, 631 (1997).
[3] V. Agranovich, *Excitations in Organic Solids* (Oxford University Press, New York, 2009).
[4] D. G. Lidzey, D. D. C. Bradley, M. S. Skolnick, T. Virgili, S. Walker, and D. M. Whittaker, Nature (London) **395**, 53 (1998).
[5] D. Lidsey, in *Thin Films and Nanostructure*, edited by V. Agranovich and G. Bassani (Elsevier, New York, 2003), Vol. 31.
[6] P. Michetti and G. C. La Rocca, Phys. Rev. B **77**, 195301 (2008).
[7] V. Agranovich and G. C. La Rocca, Solid State Commun. **135**, 544 (2005).
[8] P. Michetti and G. C. La Rocca, Phys. Rev. B **79**, 035325 (2009).
[9] R. J. Holmes and S. R. Forrest, Phys. Rev. Lett. **93**, 186404 (2004).
[10] S. Kéna-Cohen and S. R. Forrest, Phys. Rev. B **77**, 073205 (2008).
[11] M. Litinskaya, P. Reineker, and V. M. Agranovich, Phys. Status Solidi A **201**, 646 (2004).
[12] H. Zoubi and G. C. La Rocca, Phys. Rev. B **71**, 235316 (2005).
[13] S. Kéna-Cohen, M. Davanço, and S. R. Forrest, Phys. Rev. Lett. **101**, 116401 (2008).
[14] H. Kondo, Y. Yamamoto, A. Takeda, S. Yamamoto, and H. Kurisu, J. Lumin. **128**, 777 (2008).
[15] S. Kéna-Cohen, M. Davanço, and S. R. Forrest, Phys. Rev. B **78**, 153102 (2008).
[16] L. Fontanesi and G. C. La Rocca, Phys. Status Solidi C **5**, 2441 (2008).
[17] L. Fontanesi, L. Mazza, and G. C. La Rocca, Proceeding of ICPS 29, 2008 (unpublished).
[18] L. Mazza, L. Fontanesi, and G. C. La Rocca, following paper, Phys. Rev. B **80**, 235314 (2009).
[19] G. Grosso and G. Pastori Parravicini, *Solid State Physics* (Academic, New York, 2000).
[20] F. Bassani and G. Pastori Parravicini, *Electronic States and Optical Transitions in Solids* (Pergamon, New York, 1975).
[21] V. Seshadri and V. M. Kenkre, Phys. Rev. A **17**, 223 (1978).
[22] G. Panzarini, L. C. Andreani, A. Armitage, D. Baxter, M. S. Skolnick, V. N. Astratov, J. S. Roberts, A. V. Kavokin, M. R. Vladimirova, and M. A. Kaliteevski, Phys. Rev. B **59**, 5082 (1999).
[23] V. Savona, C. Piermarocchi, A. Quattropani, P. Schwendimann, and F. Tassone, Phase Transitions **68**, 169 (1999).
[24] A. Davydov, *Theory of Molecular Excitons* (Plenum, New York, 1971).
[25] J. Knoester and V. Agranovich, in *Thin Films and Nanostructure*, edited by V. Agranovich and G. Bassani (Elsevier, New York, 2003), Vol. 31.
[26] M. Schubert, Phys. Rev. B **53**, 4265 (1996).
[27] D. B. Balagurov and G. C. La Rocca, Phys. Status Solidi C **1**, 518 (2004).
[28] H. Wöhler, G. Haas, M. Fritsch, and D. A. Mlynski, J. Opt. Soc. Am. A **5**, 1554 (1988).
[29] R. J. Holmes and S. R. Forrest, Phys. Rev. B **71**, 235203 (2005).
[30] S. R. Forrest, Chem. Rev. (Washington, D.C.) **97**, 1793 (1997).